Published in final edited form as:
Radiat Res. 2010 July ; 174(1): 91–100. doi:10.1667/RR1933.1.

Computational Electromagnetic Analysis in a Human Head Model with EEG Electrodes and Leads Exposed to RF-Field Sources at 915 MHz and 1748 MHz

Leonardo M. Angelone[a,b,1], **Giorgi Bit-Babik**[c], and **Chung-Kwang Chou**[c]

[a] Division of Physics, Office of Science and Engineering Laboratories, Center for Devices and Radiological Health, U.S. Food and Drug Administration, Silver Spring, Maryland [b] Athinoula A. Martinos Center for Biomedical Imaging, Department of Radiology, Massachusetts General Hospital, Charlestown, Massachusetts [c] Enterprise Mobility Solutions, Motorola Inc., Fort Lauderdale, Florida

Abstract

An electromagnetic analysis of a human head with EEG electrodes and leads exposed to RF-field sources was performed by means of Finite-Difference Time-Domain simulations on a 1-mm^3 MRI-based human head model. RF-field source models included a half-wave dipole, a patch antenna, and a realistic CAD-based mobile phone at 915 MHz and 1748 MHz. EEG electrodes/leads models included two configurations of EEG leads, both a standard 10–20 montage with 19 electrodes and a 32-electrode cap, and metallic and high resistive leads. Whole-head and peak 10-g average SAR showed less than 20% changes with and without leads. Peak 1-g and 10-g average SARs were below the ICNIRP and IEEE guideline limits. Conversely, a comprehensive volumetric assessment of changes in the RF field with and without metallic EEG leads showed an increase of two orders of magnitude in single-voxel power absorption in the epidermis and a 40-fold increase in the brain during exposure to the 915 MHz mobile phone. Results varied with the geometry and conductivity of EEG electrodes/leads. This enhancement confirms the validity of the question whether any observed effects in studies involving EEG recordings during RF-field exposure are directly related to the RF fields generated by the source or indirectly to the RF-field-induced currents due to the presence of conductive EEG leads.

INTRODUCTION

Electroencephalography (EEG) in combination with exposure to mobile phone or equivalent sources has been used to model neurological effects of mobile phone exposure (1). However, there are some questions regarding the effect of EEG conductive leads on the RF-field exposure. When conductive EEG leads are exposed to an RF field (e.g., RF coil in MRI, mobile phones), induced currents may be generated along the leads; such currents, when conducted into the head through the interface between EEG electrode and epidermis, may be associated with changes in the RF power distribution in the anatomical structures underneath the electrode, including epidermis, fat, skull and brain (2–4). For relatively high-power RF-field sources, such as MRI RF coils (i.e., power of the order of tens of watts), changes in the RF-field power inside the head may raise thermally related safety issues (5–9), whereas for lower-power RF-field sources, such as mobile phones (i.e., power of the

[1]Address for correspondence: 10903 New Hampshire Avenue, WO62 Rm. 1109, Silver Spring, MD 20993-0002; leonardo.angelone@fda.hhs.gov.

order of hundreds of mW), the induced currents from the EEG leads into the head may affect dosimetry (10) and the proper setup for the EEG measurements (1).

Numerical studies based on the Finite-Difference Time-Domain (FDTD) method (11) have been widely used to study RF-field dosimetry (12–16) in terms of the specific absorption rate (SAR) (17). The FDTD method has been shown to provide results with a 20% accuracy compared to experimental setups (8), and it has been selected as one of the primary methods for SAR evaluation by the IEEE International Committee on Electromagnetic Safety (18).

SAR distribution in the human head is strongly affected by the inhomogeneous dielectric properties of the human head tissues (15,16,19,20); the use of numerical head models with increasing spatial resolution and anatomical detail (10,15,21,22) allowed improved precision in estimation of local SAR with respect to thin anatomical structures of the human head, including those close to the EEG electrodes such as epidermis, subcutaneous tissue and bone marrow. Simulation and experimental studies performed with medical implants or EEG leads exposed to an RF field (10,21,23,24) showed local SAR peaks near the metallic implants or EEG electrodes, with values depending on the lead orientation (10), shielding effect of EEG leads (21,25), radiofrequency (21,25), number of EEG electrodes/leads (10,21), and resistivity of EEG leads (2,3,17,26). In the present study, we performed a systematic numerical analysis of the effects of these variables on the electromagnetic field and SAR in a 1-mm^3 resolution human head model with EEG electrodes/leads and exposed to RF fields from a number of sources, including a mobile phone.

METHODS

Numerical Head Model

Anatomical MRI data were acquired on a healthy 37-year-old right-handed adult male volunteer. Informed consent was obtained in accordance with Massachusetts General Hospital policies. Data were acquired with a quadrature birdcage transmit/receive head coil on a 1.5 T scanner (General Electric, Milwaukee, WI). Data were collected with a T1-weighted 3D-SPGR sequence (TR/TE = 24/8 ms) with 124 slices, 1.3 mm thick (matrix size 256 × 192, FOV 256 mm). The volume data were resampled to isotropic voxels with dimensions of 1 × 1 × 1 mm^3. Segmentation was then applied on this dataset volume. Twenty-six non-brain anatomical structures were segmented by means of morphometric analysis.[2] Three brain structures (cerebrospinal fluid, gray and white matter) were also segmented with an automatic segmentation algorithm (27,28) and coregistered with the non-brain structures. The final head model (Fig. 1) consisted of a total of 29 anatomical structures (Table 1). Each anatomical structure was assigned biophysical properties (Table 1) at 915 and 1748 MHz, frequencies within the commonly used transmit bands for mobile phones (19,29–31). The electrical parameters were considered: (a) linear with electric field, (b) isotropic, (c) dispersive and (d) heterogeneous in space (32).

Numerical Model of RF-Field Sources

Three RF-field sources were modeled: a half-wave dipole, a patch antenna and a mobile phone.

Half-wave dipole—A dipole was modeled with a perfectly electric conductive (PEC) 164-mm-long wire, placed 15 mm between the feedpoint and head surface (Fig. 1). The dipole was center-fed, and simulations were performed at 915 MHz.

[2]L. M. Angelone, *RF Dosimetry At Ultra High-Field MRI*. Ph.D. Dissertation, Biomedical Engineering Department, Tufts University, Medford, MA, 2008.

Patch antenna—A patch antenna was modeled as in ref. (10) using a rectangular block (192 × 136 mm^2, 10 mm thick) 61 mm from the head. The patch was composed of a dielectric material (σ = 0.0001 S/m, ε_r = 1.5), placed between a ground plate (192 × 136 mm^2) of perfectly conductive material on one side and a metallic resonant plate (140 × 90 mm^2) on the other side, facing the head (Fig. 1). The two copper plates were connected with a thin metallic wire, where a 915 MHz sinusoidal source was placed.

Mobile phone—A CAD model of a commercially available mobile phone was used. The distance between head and feedpoint of the phone was 15 mm, as for the dipole. The minimum distance between the phone and the head was 3 mm. Simulations with the phone were performed at 915 MHz and 1748 MHz.

Numerical Model of EEG Electrodes and Leads

EEG electrodes—Thirty-two EEG electrodes were designed with Circuit Maker (Altium Inc., San Diego, CA) on a 2D mask and imported into Matlab (Mathworks, Natick, MA) (26). The mask was coregistered with the axial slice of the largest diameter on the head model. EEG electrodes present in the mask were projected and placed on top of the surface of the head model ("epidermis" of the model). EEG electrodes were modeled as discs (radius = 7 mm, height = 3 mm). The model was then imported into the XFDTD software (Remcom Co., State College, PA) to complete the model by including the EEG leads. Two different types of EEG caps were modeled (Fig. 1): Set 1 and Set 2.

Set 1—EEG leads modeled as PEC wires were connected separately to each electrode and were oriented around the head (Set 1 in Fig. 1) (10,21,25). Leads were modeled using three to nine segments, depending on the position with respect to the head, with distance from the head between 1 mm and 11 mm. Two different subsets were simulated to model two typical configurations of connections between EEG electrodes and amplifier through conductive leads: 19 leads, following the standard 10–20 montage (33), and an extended 32-lead configuration (35–37). For this set, the case of leads with increased resistivity (ρ = 0.01 Ωm) was also evaluated for comparison (26,35).

Set 2—Thirty-two leads connecting to each electrode and following the head curvature, never touching the head surface, were bundled at the Cz position (33,35,37), exiting vertically from the head for 53 mm (Set 2 in Fig. 1).

FDTD Simulations

FDTD simulations were performed using commercially available software (XFDTD, Remcom Inc., State College, PA). The models were imported into the XFDTD software, and a uniform padding of 40 free-space cells with seven layers of perfectly matching (PML) boundary was used to model open space beyond the simulation domain. A harmonic source (1 V peak-to-peak, 50 Ω feedpoint resistance) was used to model the RF-field excitation in all cases. Calculations were run until steady-state conditions were reached with −40 dB of convergence criterium as evaluated with the XFDTD software, corresponding to approximately 12 cycles of sinusoidal signal. Simulations were performed on a Dual Core 1.83 GHz computer with 4 GB of RAM. Electric-field amplitude, induced currents, 1-g average (SAR_{1g}), 10-g average (SAR_{10g}), and whole-head average SAR (SAR_w) were computed with the XFDTD software (38). The results were normalized to 0.25 W of net input power at 915 MHz and 0.125 W at 1748 MHz.

The SARs calculated with EEG electrodes/leads were compared voxel by voxel (i.e., 1-mm^3 spatial resolution) to the corresponding values calculated without EEG electrodes as follows (26):

$$P_i = \frac{SAR_i^{LEAD}}{SAR_i^{NOLEAD}} = \frac{Power_i^{LEAD}}{Power_i^{NOLEAD}} \quad (1)$$

where SAR_i^{LEAD} and SAR_i^{NOLEAD} are the SARs in the *i*th voxel with or without EEG electrodes/leads, respectively. This ratio is equivalent to the ratio of the RF-field power absorbed in the *i*th voxel with or without EEG electrodes/leads, respectively.

RESULTS

The RF field induced visible currents along the EEG leads for both sets with all RF-field sources modeled (Fig. 2) with related SAR increases underneath the EEG electrodes (Fig. 3).

Volumetric Analysis of Changes in SAR

Table 2 reports the volumetric analysis as described in Eq. (1) for different anatomical structures present underneath the EEG electrodes, namely epidermis, subcutaneous fat, skull (i.e., outer and inner table of skull), bone marrow and brain (i.e., gray and white matter). Figure 4 shows cross sectional views of the P_i patterns for Set 1 and Set 2. The largest increase of 1279-fold was in the epidermis with Set 1 exposed to the dipole. Local changes in the brain were observed with Set 1 with the dipole [i.e., max (P_i) = 46, avg (P_i) = 1.2 and 5% of brain volume with $P_i > 2$] and patch antenna [i.e., max (P_i) = 21, avg (P_i) = 1 and 4% of brain volume with $P_i > 2$]. For the mobile phone at 915 MHz (Table 2 and Fig. 4), there was a peak increase of 859-fold in the epidermis and 48-fold in the brain with Set 1 and 14% of brain volume wih $P_i > 2$. Smaller changes were observed with the mobile phone at 1748 MHz, with a 52-fold maximum increase in the epidermis, 14-fold in the brain, and 4% of brain volume with $P_i > 2$. The enhancements for Set 2 were all smaller than those for Set 1. For example, for exposure to the mobile phone at 915 MHz, there was a peak increase of 460-fold in the epidermis but smaller changes in the internal structures, with a 6.6-fold peak increase and 0.8% $P_i > 2$ in the brain structures.

Antenna Performance and Peak SAR Evaluation

For both head models with EEG leads and with all RF-field sources at 915 MHz there were no significant changes in antenna performance (i.e., efficiency, impedance at source) and whole-head average SAR (Table 3).

Dipole

There was a 13% increase in peak 1-g average SAR and a 14% increase in peak 10-g average SAR with electrode Set 1 compared to the case of no electrodes/leads. No changes (<1%) in peak 1-g average and 10-g average were observed with Set 2 (Table 3). The peak SAR was on the epidermis under the EEG lead near the dipole (see Fig. 3) for Set 1, whereas it was in the epidermis at the Cz position, where the leads were bundled, for Set 2.

Patch

There was a 2.4× increase in peak 1-g average and 20% in peak 10-g average SAR with Set 1 compared to the case of no electrodes/leads. No changes (<1%) in peak 1-g average and 10-g average were observed with Set 2 (Table 3).

Mobile Phone

There was a 5% increase in the peak 1-g average and 20% in the peak 10-g average SAR with Set 1 compared to the case with no electrodes/leads. No changes were observed with Set 2 (Table 3). Similar to the dipole and patch antenna cases, the peak was in the epidermis under the EEG electrode closest to the source for Set 1, whereas it was at the Cz position for Set 2 (see Fig. 3). Overall, the effects of EEG leads were reduced at 1748 MHz (Table 3) compared to 915 MHz. There was a 10% increase in peak 1-g average and 10-g average SAR with Set 1 and 4% with Set 2 compared to the case of no electrodes/leads. The peak SARs were similar for 19 and 32 electrodes/leads (Table 4). As for the 32 electrodes, the peaks SARs for 19 electrodes were under the EEG electrode/leads closest to the source. Table 5 shows changes within 10% for peak 1-g average and 10-g average SAR with high resistive leads compared to the no-lead case. The effect of increased resistivity was more evident for Set 1, with a peak 10-g average SAR of 0.49 W/kg compared to 0.54 W/kg with conductive leads (Table 3) and 0.44 W/kg without leads.

DISCUSSION

When conductive leads are exposed to a radiofrequency field, induced currents are generated along the leads (2). The effects of such induced currents can be seen in two perspectives: (a) potential safety issues related to local increase of electric-field deposition at the interface between the EEG electrode and the human head, historically measured in terms of specific absorption rate (17) and (b) effects on electromagnetic-field distribution related to the EM scattering of the leads; i.e., the EEG leads cannot be considered proper “RF-transparent” measurement probes. In this perspective, changes in the EMF due to the EEG leads can be considered as “noise” with respect to the measurements of EEG for RF-field exposure of a specific antenna. Schmid *et al.* (10) presented a new exposure system for studies requiring EEG recording on human subjects exposed to GSM900-and UMTS-equivalent sources. Although the study showed minimal interference when EEG leads were placed orthogonally to the source, the study raised potential issues for different lead orientations or numbers of EEG electrodes/leads. Since the amount of current induced depends on the frequency and the specific geometry of the leads with respect to the source, estimation of such currents can be cumbersome for complex geometries, such as conductive leads placed on the head of human subjects during electroencephalography recordings. In such cases, an anatomically precise computational model can be useful to evaluate the interactions between the leads and the RF-field source. Several MRI-based human head models are now available (15). The model used in this study is characterized by a 1-mm^3 isotropic spatial resolution and 29 anatomical structures, which allowed the modeling with geometrical accuracy the thin structures of interests for the problem of EEG leads, such as epidermis, where EEG electrodes are connected to the head, and bone marrow, where potential local increases in SAR are possible (21).

Previous studies used peak 1-g average and 10-g average SAR to evaluate changes in SAR with EEG leads exposed an RF field generated by mobile phones (10,25). The regulatory limit for localized exposure to an RF field generated by mobile phones set by the Federal Communications Commission (FCC) is 1.6 W/kg for peak 1-g average SAR (39,40). The limit set by the International Commission on Non-Ionizing Radiation Protection (ICNIRP) (41) and the American National Standard Institute (ANSI) and IEEE (42) is 2 W/kg for peak 10-g average SAR. It has been shown that the temperature rise in tissue correlates well with an average tissue mass of 10 g (43,44). This study showed that the peak 1-g average and peak 10-g average SARs with mobile phones were below the corresponding exposure limits. Thus, given the relatively low input power of mobile phones as opposed, for example, to the RF coil used in MRI (21), the conductive EEG leads are not expected to generate excessive temperature rises during exposure to the RF field of mobile phones.

The whole-head average SAR and 10-g average SAR did not vary significantly (i.e., less than 10%) in the different cases considered. The peak 1-g average SAR varied less than 10% with dipole and mobile phone, while a twofold change compared to the case of no leads was observed with Set 1 and the patch antenna. The results of the study confirmed the peculiar local behavior of RF power in the presence of conductive leads (45), with changes occurring in volumes of a few mm^3 rather than over the whole head. While relatively coarse parameters such as whole-head average SAR, 10-g average SAR or even 1-g average SAR did not show significant changes in the RF-field power with and without leads, a more comprehensive volumetric assessment of changes in RF power over the entire head showed significant local increases of RF-field energy absorption in anatomical structures underneath the EEG electrodes.

The resolution of the numerical model used in this study is one of the highest among the anthropomorphic numerical models for RF-field dosimetry (15); this allowed a 1-mm^3-resolution volumetric assessment of RF-field power. Numerical errors related to staircasing of small structures may still be present (8,46), and a proper validation of these results with geometrically matched experimental measurements may be needed. The SARs found in this study were in line with previous published work. The simulations with the dipole and mobile phone were in line with canonical results.[3] The peak 10-g average SAR with the patch antenna and the head model without leads was 1.2 W/kg (1 W of net input power), similar to the value of 1.02 W/kg simulated and 0.92 W/kg measured with an antenna of same dimensions and at the same distance from the head reported in ref. (10). Simulations with a mobile phone at 915 MHz and a head model without leads resulted in a peak 10-g average of 1.77 W/kg (1 W of net input power) compared to 3.4 W/kg in ref. (15). Since the study in ref. (15) was performed with the SAM phantom, for a more direct comparison, simulations with an electrically homogeneous model ($\sigma = 0.97$ S/m, $\varepsilon_r = 55.6$, $\rho = 1040$ kg m^{-3}) (19,29) based on the same head model used in this study were performed with the mobile phone at 915 MHz. The peak 10-g average SAR for this homogeneous model was 3.18 W/kg (1 W of net input power), within 10% of the value in ref. (15).

Our simulations showed that the presence of conductive EEG leads combined with specific configurations of an RF-field source created a reduction of the RF field (i.e., “shielding effect”) in anatomical structures near the EEG electrodes, similar to that reported in refs. (21) and (25). In particular, the value of P_i was less than one in the epidermis or bone marrow with the dipole at 915 MHz. The shielding effect was greater with the patch antenna. The results of this study also confirm that the leads with higher resistivity ($\rho = 0.01$ Ωm), used in previous studies to minimize interactions with other RF-field sources (35), helped reduce the currents induced in the leads and the related local SAR on the epidermis and surrounding structures.

CONCLUSIONS

A 1-mm^3 anatomically precise human head model with two realistic sets of EEG electrodes and leads was used to evaluate potential changes in SAR during exposure to several RF-field sources, including a mobile phone. Significant changes induced by the conductive EEG leads at the electrode sites with respect to the control case of a human head without EEG leads. Observed SAR peaks were below exposure limits, suggesting that no potential thermal issues may be present when using EEG leads with a mobile phone or equivalent source. However, local enhancement of the electromagnetic field and SAR over those

[3]M. Siegbahn, G. Bit-Babik, J. Keshvari, A. Christ, B. Derat, V. Monebhurrun, C. Penney and T. Wittig, An international inter-laboratory comparison of mobile phone SAR calculation with CAD-based models. In *Abstracts of the Bioelectromagnetics Society Annual Meeting*, p. 22, Davos, Switzerland, 2009.

without leads was present over the entire head, including gray and white matter structures. Changes in the SAR were different for two realistic configurations of EEG caps and were present for both the standard 10–20 montage and the extended 32-EEG electrodes. High-resistive leads reduced the currents induced in the leads and local SAR in the head.

The results of this study indicate that the effect of RF-field exposure on EEG is not a simple issue to resolve. Since EEG recording measures very small electrical variations in the brain, it is important to realize that an induced current is carried by the conductive leads into the head. Whether any observed effect is directly related to the RF fields or is caused indirectly by the current induced by the RF field due to the presence of conductive EEG leads must be determined to understand the biological effects of RF-field exposure.

Acknowledgments

This study was supported by the Mobile Manufacturer Forum, the NCRR (grant P41RR14075), the MIND Institute, and the Athinoula A. Martinos Center for Biomedical Imaging. Giorgi Bit-Babik and C-K. Chou are employees of Motorola whose research focuses on the safe use of electromagnetic energy. They contributed their time on this project with the support of the company. The authors would like to thank Bruce Rosen, Giorgio Bonmassar, Christos Vasios, Nikos Makris, David Kennedy, Jonathan Kaiser, George Papadimitriou at the A. Martinos Center for Biomedical Imaging and Mark Cronin-Golomb and Sergio Fantini at Tufts University for the help and the useful insights during the completion of the study. The mention of commercial products, their sources, or their use in connection with material reported herein is not to be construed as either an actual or implied endorsement of such products by the Department of Health and Human Services.

References

1. Valentini E, Curcio G, Moroni F, Ferrara M, De Gennaro L, Bertini M. Neurophysiological effects of mobile phone electromagnetic fields on humans: a comprehensive review. Bioelectromagnetics 2007;28:415–432. [PubMed: 17503518]
2. Guy AW. Biophysics – Energy absorption and distribution. AGARD Lect Ser 1974;78:1–14.
3. Chou CK, Guy AW. Carbon-loaded Teflon electrodes for chronic EEG recordings in microwave research. J Microwave Power 1979;14:399–404.
4. Chou, CK. RF heating of metallic implants during MRI. In: Ng, K-H.; Montgomery, ND.; Tan, L-K., editors. International EMF Conference 2007: Electromagnetic Fields, Bioeffects Research, Medical Applications, and Standards Harmonization. University of Malaysia Press; Kuala Lumpur: 2008. p. 30-37.
5. Ibrahim TS, Kangarlu A, Chakeress DW. Design and performance issues of RF coils utilized in ultra high field MRI: experimental and numerical evaluations. IEEE Trans Biomed Eng 2005;52:1278–1284. [PubMed: 16041991]
6. Collins CM, Liu W, Wang J, Gruetter R, Vaughan JT, Ugurbil K, Smith MB. Temperature and SAR calculations for a human head within volume and surface coils at 64 and 300 MHz. J Magn Reson Imaging 2004;19:650–656. [PubMed: 15112317]
7. Finelli DA, Rezai AR, Ruggieri PM, Tkach JK, Nyenhuis JA, Hrdlicka G, Sharan A, Gonzalez-Martinez J, Stypulkowski PH, Shellock FG. MR imaging-related heating of deep brain stimulation electrodes: in vitro study. Am J Neuroradiol 2002;23:1795–1802. [PubMed: 12427641]
8. Gajsek P, Walters TJ, Hurt WD, Ziriax JM, Nelson DA, Mason PA. Empirical validation of SAR values predicted by FDTD modeling. Bioelectromagnetics 2002;23:37–48. [PubMed: 11793404]
9. Shellock, FG. Reference Manual for Magnetic Resonance Safety, Implants and Devices. Biomedical Research Publishing Group; Los Angeles: 2008.
10. Schmid G, Cecil S, Goger C, Trimmel M, Kuster N, Molla-Djafari H. New head exposure system for use in human provocation studies with EEG recording during GSM900- and UMTS-like exposure. Bioelectromagnetics 2007;28:636–647. [PubMed: 17654486]
11. Taflove, A.; Hagness, SC. Computational Electrodynamics: The Finite-Difference Time-Domain Method. Artech House; Boston: 2000.

12. Collins CM, Li S, Smith MB. SAR and B1 field distributions in a heterogeneous human head model within a birdcage coil. Magn Reson Med 1998;40:847–856. [PubMed: 9840829]
13. Ibrahim TS, Mitchell C, Abraham R, Schmalbrock P. In-depth study of the electromagnetics of ultrahigh-field MRI. NMR Biomed 2007;20:58–68. [PubMed: 17006885]
14. Bit-Babik G, Guy AW, Chou CK, Faraone A, Kanda M, Gessner A, Wang J, Fujiwara O. Simulation of exposure and SAR estimation for adult and child heads exposed to radiofrequency energy from portable communication devices. Radiat Res 2003;163:580–590. [PubMed: 15850420]
15. Kainz W, Christ A, Kellom T, Seidman S, Nikoloski N, Beard B, Kuster N. Dosimetric comparison of the specific anthropomorphic mannequin (SAM) to 14 anatomical head models using a novel definition for the mobile phone positioning. Phys Med Biol 2005;50:3423–3445. [PubMed: 16177519]
16. Gandhi OP, Chen XB. Specific absorption rates and induced current densities for an anatomy-based model of the human for exposure to time-varying magnetic fields of MRI. Magn Reson Med 1999;41:816–823. [PubMed: 10332859]
17. NCRP. Report No. 67. National Council on Radiation Protection and Measurements; Bethesda, MD: 1981. Radiofrequency Electromagnetic Fields: Properties, Quantities and Units, Biophysical Interaction, and Measurement.
18. Standard P1528. 1-201x, IEEE, Draft, SCC-34, SC-2, WG-2 Computational Dosimetry. IEEE; New York: 2009. Draft Recommended Practice for Determining the Peak Spatial-Average Specific Absorption Rate (SAR) in the Human Body from Wireless Communications Devices, 30 MHz–6 GHz: General Requirements for using the Finite Difference Time Domain (FDTD) Method for SAR Calculations.
19. Gabriel C, Gabriel S, Corthout E. The dielectric properties of biological tissues: I. Literature survey. Phys Med Biol 1996;41:2231–2249. [PubMed: 8938024]
20. IEEE. Clause 5: Phantom models Standard. Vol. 1528. IEEE; New York: 2003. Recommended Practice for Determining the Peak Spatial-Average Specific Absorption Rate (SAR) in the Human Head from Wireless Communications Devices: Measurement Techniques.
21. Angelone L, Potthast A, Segonne F, Iwaki S, Belliveau J, Bonmassar G. Metallic electrodes and leads in simultaneous EEG-MRI: Specific absorption rate (SAR) simulation studies. Bioelectromagnetics 2004;25:285–295. [PubMed: 15114638]
22. Makris N, Angelone L, Tulloch S, Sorg S, Kaiser J, Kennedy D, Bonmassar G. MRI-based anatomical model of the human head for specific absorption rate mapping. Med Biol Eng Comput 2008;46:1239–1251. [PubMed: 18985401]
23. Ho HS. Safety of metallic implants in magnetic resonance imaging. J Magn Reson Imaging 2001;14:472–477. [PubMed: 11599073]
24. Chou CK, McDougall JA, Chan KW. RF heating of implanted spinal fusion stimulator during magnetic resonance imaging. IEEE Trans Biomed Eng 1997;44:367–73. [PubMed: 9125821]
25. Hamblin DL, Anderson V, McIntosh RL, McKenzie RJ, Wood AW, Iskra S, Croft RJ. EEG electrode caps can reduce SAR induced in the head by GSM900 mobile phones. IEEE Trans Biomed Eng 2007;54:914–920. [PubMed: 17518289]
26. Angelone LM, Vasios CE, Wiggins G, Purdon PL, Bonmassar G. On the effect of resistive EEG electrodes and leads during 7 T MRI: simulation and temperature measurement studies. Magn Reson Imaging 2006;24:801–812. [PubMed: 16824975]
27. Dale AM, Fischl B, Sereno MI. Cortical surface-based analysis. I. Segmentation and surface reconstruction. Neuroimage 1999;9:179–194. [PubMed: 9931268]
28. Segonne F, Dale AM, Busa E, Glessner M, Salat D, Hahn HK, Fischl B. A hybrid approach to the skull stripping problem in MRI. Neuroimage 2004;22:1060–1075. [PubMed: 15219578]
29. Federal Communications Commission (FCC). Body Tissue Dielectric Parameters Tool. [Available online at http://www.fcc.gov/fcc-bin/dielec.sh]
30. Li QX, Gandhi OP. Thermal implications of the new relaxed IEEE RF safety standard for head exposures to cellular telephones at 835 and 1900 MHz. IEEE Trans Microwave Theory Tech 2006;54:3146–3154.

31. DeMarco SC, Lazzi G, Liu W, Weiland JD, Humayun MS. Computed SAR and thermal elevation in a 0.25-mm 2-D model of the human eye and head in response to an implanted retinal stimulator – part I: models and methods. IEEE Trans Antennas Propagation 2003;51:2274–2285.
32. Vorst, AV.; Rosen, A.; Kotsuka, Y. RF/Microwave Interaction with Biological Tissues. Wiley; New York: 2006.
33. Klem GH, Luders HO, Jasper HH, Elger C. The ten-twenty electrode system of the international federation of clinical neurophysiology. Electroencephalogr Clin Neurophysiol 1999;(Suppl 52):3–6.
34. Mullinger K, Debener S, Coxon R, Bowtell R. Effects of simultaneous EEG recording on MRI data quality at 1.5, 3 and 7 Tesla. Int J Psychophysiol 2008;67:178–188. [PubMed: 17689767]
35. Vasios CE, Angelone LM, Purdon PL, Ahveninen J, Belliveau JW, Bonmassar G. EEG/(f)MRI measurements at 7 Tesla using a new EEG cap ("InkCap"). Neuroimage 2006;33:1082–1092. [PubMed: 17035045]
36. Lemieux L, Allen PJ, Franconi F, Symms MR, Fish DR. Recording of EEG during fMRI experiments: patient safety. Magn Reson Med 1997;38:943–952. [PubMed: 9402196]
37. Regan, D. Human Brain Electrophysiology: Evoked Potentials and Evoked Magnetic Fields in Science and Medicine. Elsevier; New York: 1989.
38. Caputa K, Okoniewski M, Stuchly MA. An algorithm for computations of the power deposition in human tissue. IEEE Antennas Propagation Mag 1999;41:102–107.
39. Federal Communications Commission (FCC) Office Engineering Technologies. OET Bull. Vol. 65. Washington, DC: 2001. Evaluating Compliance with FCC Guidelines for Human Exposure to Radiofrequency Electromagnetic Fields.
40. American National Standard Institute (ANSI). American National Standard Safety Levels with respect to Human Exposure to Radio Frequency Electromagnetic Fields, 300 kHz to 100 GHz. Standard C95.1. 1982
41. International Commission on Non-Ionizing Radiation Protection (ICNIRP). Guidelines for limiting exposure to time-varying electric, magnetic, and electromagnetic fields (up to 300 GHz). Health Phys 1998;74:494–522. [PubMed: 9525427]
42. American National Standard Institute (ANSI)/IEEE. 3 kHz to 300 GHz. Standard C95.1. IEEE; New York: 2006. Standard for Safety Levels with Respect to Human Exposure to Radio Frequency Electromagnetic Fields.
43. Hirata A, Shirai K, Fujiwara O. On averaging mass of SAR correlating with temperature evaluation due to a dipole antenna. Prog Electromagn Res 2008;84:221–237.
44. McIntosh RI, Anderson V, McKenzie RJ. The use of temperature as a metric for the assessment of RF safety. Radiat Prot Australasia 2008;25:9–21.
45. Bassen H, Kainz W, Mendoza G, Kellom T. MRI-induced heating of selected thin wire metallic implants –laboratory and computational studies – findings and new questions raised. Minim Invasive Ther Allied Technol 2006;15:76–84. [PubMed: 16754190]
46. Railton CJ, Schneider JB. An analytical and numerical analysis of several locally conformal FDTD schemes. IEEE Trans Microwave Theory Tech 1999;47:56–66.

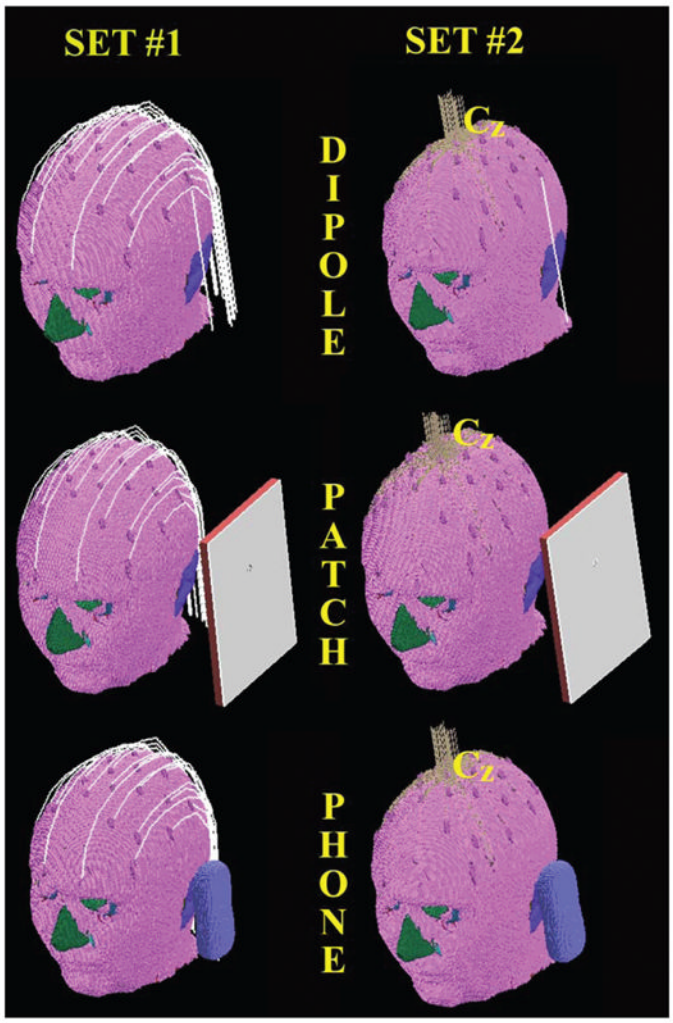

FIG. 1.

Three-dimensional view of MRI-based human head model wearing EEG electrodes/leads used for the study. The models of the three RF-field sources used (dipole, patch antenna and mobile phone) are shown. Thirty-two EEG electrodes with two realistic configurations of EEG leads (Set 1 and Set 2) were evaluated.

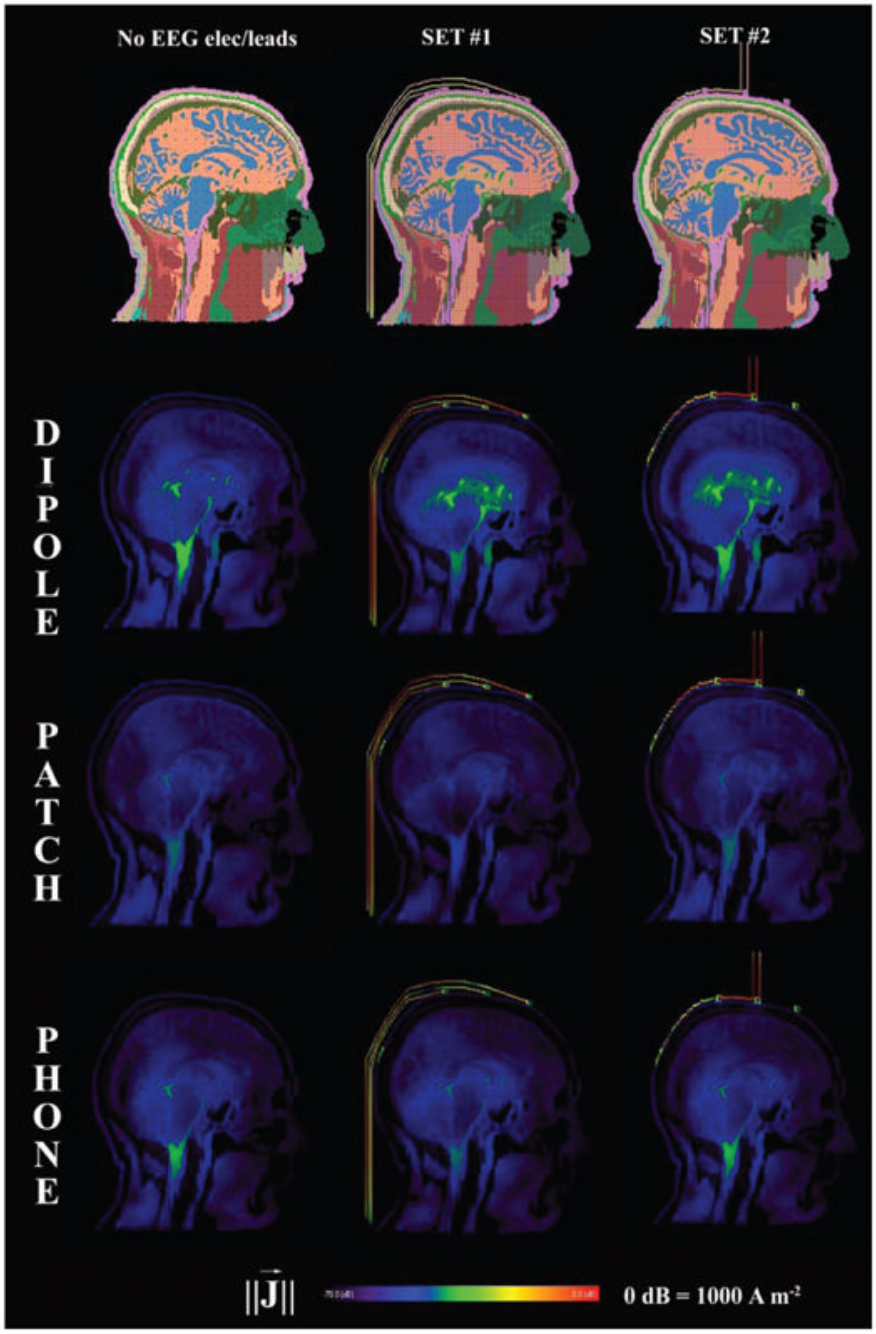

FIG. 2.

Sagittal view of induced currents for the control case (no leads) and the two sets of EEG electrodes/leads. The sources were a half-wave dipole antenna, a patch antenna and a mobile phone at 915 MHz. Values are normalized for 0.25 W of available input power. The induced currents along the conductive leads are visible. Color scale from 0 dB to −70 dB.

FIG. 3.

Coronal view of SAR for the control case (no leads) and the two sets of EEG electrodes/leads. The sources were a half-wave dipole antenna, a patch antenna and a mobile phone at 915 MHz. All sources were on the left of the head (i.e., right in the image as for radiological convention). Values normalized for 0.25 W of available input power. Arrows indicate local increases in SAR underneath the EEG electrodes.

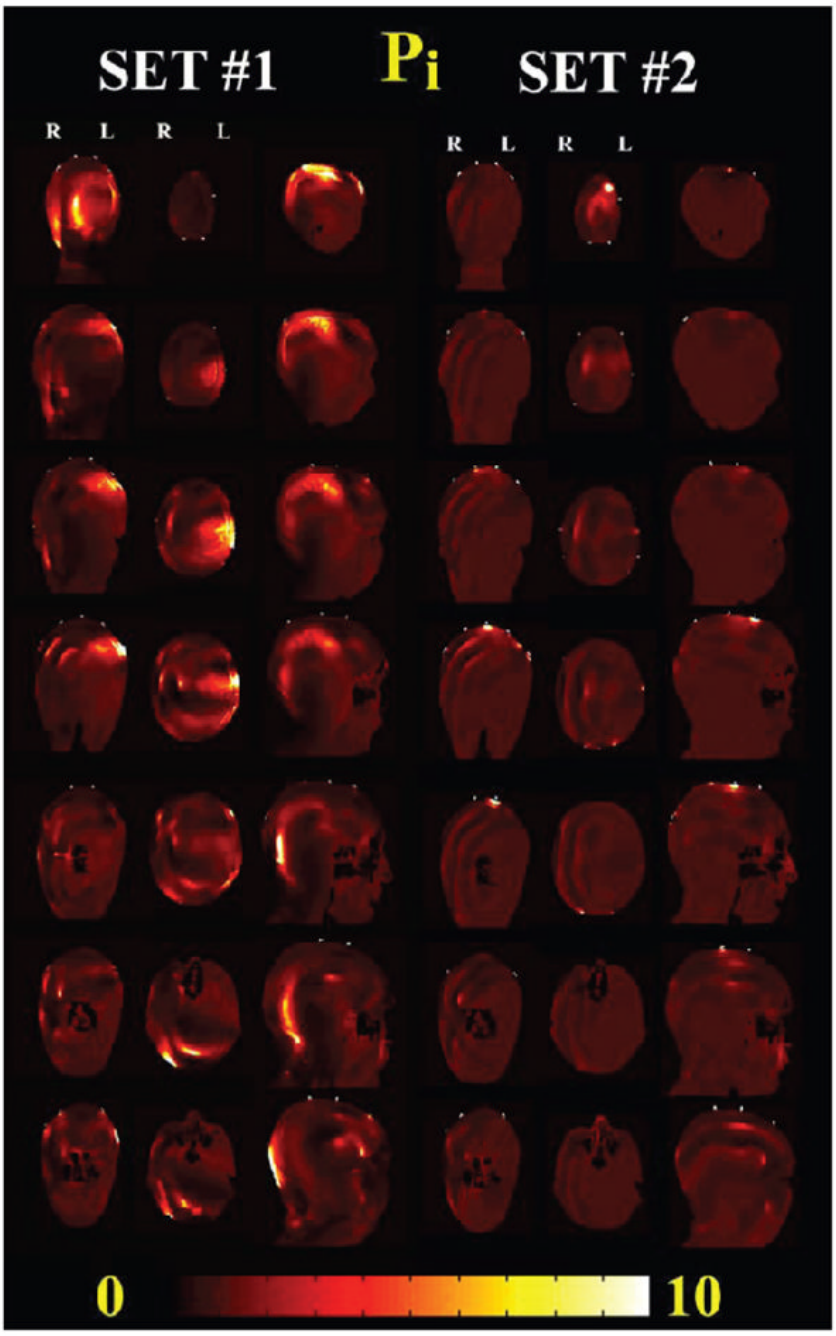

FIG. 4.

Changes in RF-field power with and without leads (P_i) for 915 MHz mobile phone exposure with the two sets of EEG electrodes/leads modeled. Coronal (from the back to the front of the head), axial (from the top of the head to the neck), and sagittal (from right to the left of the head) are shown. The phone was placed on the left of the head. Significant increases in P_i were observed for Set 1 near the EEG leads and in all the anatomical structures underneath the EEG electrode near the source (coronal and axial view) and on the back of the head near the leads (sagittal view). Changes for Set 2 were localized mainly underneath the electrode in Cz position, where the leads were bundled.

Radiat Res. Author manuscript; available in PMC 2011 July 1.

TABLE 1

Anatomical Structures of MRI-Based Head Model and Electrical Properties at 915 MHz and 1748 MHz

		915 MHz[d]		1748 MHz[d]	
Anatomical structural entities	**Density (kg/m^3)**	**σ (S/m)**	**ε_r**	**σ (S/m)**	**ε_r**
Brain					
Gray matter	1030[a]	0.94	52.72	1.36	50.19
White matter	1030[a]	0.59	38.88	0.89	37.09
Cerebrospinal fluid	1010[a]	2.41	68.63	2.89	67.28
Non-brain					
Adipose	920[a]	0.11	11.33	0.18	11.04
Air (respiration/digestion/sinus)	1.3[b]	0.00	1.00	0.00	1.00
Aqueous humor	1010[a,c]	1.64	68.90	2.00	68.60
Bone (facial)	1850[b]	0.14	12.45	0.27	11.81
Connective tissue	1100[a]	0.78	42.65	1.25	40.34
Cornea	1076[c]	1.39	55.23	1.83	52.87
CSF subarachnoid	1010[a]	2.41	68.63	2.89	67.28
Bone marrow	1080[b]	0.34	20.79	0.57	19.41
Dura	1030[a]	0.96	44.42	1.29	42.97
Ear/pinna	1100[a]	0.78	42.65	1.25	40.34
Epidermis	1100[a]	0.86	41.40	1.16	38.96
Inner table (skull)	1850[b]	0.14	12.45	0.27	11.81
Lens	1100[c]	0.79	46.57	1.12	45.41
Muscle	1040[d]	0.97	55.96	1.36	54.51
Nasal structures	1100[a]	0.78	42.65	1.25	40.34
Nerve	1040[a]	0.57	32.53	0.83	30.93
Orbital fat	920[a]	0.11	11.33	0.18	11.04
Outer table (skull)	1850[b]	0.14	12.45	0.27	11.81

		915 MHz[d]		1748 MHz[d]	
Anatomical structural entities	**Density (kg/m^3)**	**σ (S/m)**	**ε_r**	**σ (S/m)**	**ε_r**
Retina/choroid/sclera	1170[a]	1.17	55.27	1.57	53.65
Soft tissue	1100[a]	0.78	42.65	1.25	40.34
Spinal cord	1040[a]	0.57	32.53	0.83	30.93
Subcutaneous tissue	1100[a]	0.78	42.65	1.25	40.34
Subcutaneous fat	920[a]	0.11	11.33	0.18	11.04
Teeth	1850[b]	0.14	12.45	0.27	11.81
Tongue	1040[d]	0.97	55.96	1.36	54.51
Vitreous humor	1010[a,c]	1.64	68.90	2.00	68.60

[a] Ref. (30).

[b] Ref. (6).

[c] Ref. (31).

[d] Ref. (19).

TABLE 2

Peak and Mean Changes in RF-Field Power with and without Leads

		P_i				
	Dipole 915 MHz	**Epidermis, dermis**	**Subcutaneous fat**	**Skull**	**Bone marrow**	**Brain**
Set 1	max (P_i)	1279.0	80.8	66.2	18.8	45.9
	mean (P_i)	0.78	1.05	1.04	0.89	1.16
	Volume (1 mm^3)	16990	25348	23546	6988	70193
	$P_i > 2$					
	Volume with $P_i > 2$ percentage of total volume	4.4%	6.6%	7.3%	5.1%	5.1%
Set 2	max (P_i)	366.0	75.0	54.9	14.8	9.1
	mean (P_i)	0.81	1.05	1.07	1.01	1.03
	Volume (1 mm^3)	7163	8764	12718	3960	18485
	$P_i > 2$					
	Volume with $P_i > 2$ percentage of total volume	1.9%	2.3%	3.9%	2.9%	1.3%
	Patch 915 MHz	P_i				
		Epidermis, dermis	Subcutaneous fat	Skull	Bone marrow	Brain
Set 1	max (P_i)	270.0	163.2	8.5	10.0	21.1
	mean (P_i)	0.69	0.99	0.92	0.86	1.00
	Volume (1 mm^3)	9276	17612	13472	3744	56905
	$P_i > 2$					
	Volume with $P_i > 2$ percentage of total volume	2.4%	4.6%	4.2%	2.7%	4.1%
Set 2	max (P_i)	430.7	83.6	58.0	16.6	23.5
	mean (P_i)	0.77	1.03	1.05	1.02	0.98
	Volume (1 mm^3)	5650	9799	11075	3849	10061
	$P_i > 2$					
	Volume with $P_i > 2$ percentage of total volume	1.5%	2.6%	3.4%	2.8%	0.7%
	Mobile phone 915 MHz	P_i				
		Epidermis, dermis	Subcutaneous fat	Skull	Bone marrow	Brain

Radiat Res. Author manuscript; available in PMC 2011 July 1.

		P_i				
	Dipole 915 MHz	**Epidermis, dermis**	**Subcutaneous fat**	**Skull**	**Bone marrow**	**Brain**
Set 1	max (P_i)	859.1	454.0	31.0	21.9	47.8
	mean (P_i)	1.04	1.34	1.33	1.27	1.36
	Volume (1mm^3)	25922	41755	43417	19549	195016
	$P_i > 2$					
	Volume with $P_i > 2$ percentage of total volume	6.7%	10.9%	13.4%	14.3%	14.2%
Set 2	max (P_i)	459.5	83.9	34.5	8.2	6.6
	mean (P_i)	0.87	1.07	1.04	1.03	1.01
	Volume (1 mm^3)	7983	8698	8691	3675	11603
	$P_i > 2$					
	Volume with $P_i > 2$ percentage of total volume	2.1%	2.3%	2.7%	2.7%	0.8%
	Mobile Phone 1748 MHz	P_i				
		Epidermis, dermis	Subcutaneous fat	Skull	Bone marrow	Brain
Set 1	max (P_i)	52.2	15.9	10.2	5.3	14.1
	mean (P_i)	0.89	1.3	1.10	1.13	1.08
	Volume (1 mm^3)	26826	40065	17791	8315	56447
	$P_i > 2$					
	Volume with $P_i > 2$ percentage of total volume	7.0%	10.5%	5.5%	6.1%	4.1%
Set 2	max (P_i)	31.0	8.9	9.0	2.2	7.2
	mean (P_i)	0.74	1.0	1.00	0.97	0.98
	Volume (1mm^3)	2276	2614	3331	91	5505
	$P_i > 2$					
	Volume with $P_i > 2$ percentage of total volume	0.6%	0.7%	1.0%	0.1%	0.4%

Notes. Values for Set 1 and Set 2 for anatomical structures underneath EEG electrodes are shown. The volume with P_i higher than 2 (i.e. over 100% increase in RF power compared to no leads) is provided as the absolute value as well as a percentage of the overall volume of the anatomical structure.

TABLE 3

Dipole Patch and Mobile Phone at 915 MHz and 1748 MHz for Head without Leads and with Two Sets of 32 EEF Electrodes/Leads Modeled in this Study

Dipole - 915 MHz			
	Head no electrodes	**Set 1 32 electrodes/leads**	**Set 2 32 electrodes/leads**
Net input power (W)	0.25	0.25	0.25
Power dissipated (W)	0.18	0.18	0.18
Radiation efficiency	28.8%	26.2%	29.2%
Impedance (Z)	55.65 + j42.62	54.83 + j46.34	55.07 + j42.73
Peak 1 g average SAR (W/kg)	1.72	1.94	1.73
Peak 10 g average SAR (W/kg)	1.20	1.37	1.22
Whole-head SAR (W/kg)	0.035	0.036	0.034
Patch - 915 MHz			
	Head no electrodes	Set 1 32 electrodes/leads	Set 2 32 electrodes/leads
Net input power (W)	0.25	0.25	0.25
Power dissipated (W)	0.13	0.14	0.13
Radiation efficiency	49.2%	45.4%	49.5%
Impedance (Z)	2.68 + j30.89	2.12 + j30.58	2.63 + j30.98
Peak 1 g average SAR (W/kg)	0.54	1.29	0.54
Peak 10 g average SAR (W/kg)	0.31	0.37	0.31
Whole-head SAR (W/kg)	0.022	0.023	0.022
Mobile phone - 915 MHz			
	Head no electrodes	Set 1 32 electrodes/leads	Set 2 32 electrodes/leads
Net input power (W)	0.25	0.25	0.25
Power dissipated (W)	0.19	0.21	0.19
Radiation efficiency	21.9%	17.1%	22.1%
Impedance (Z)	64.08 + j124.33	68 + j129.35	64.11 + j124.12
Peak 1 g average SAR (W/kg)	0.82	0.86	0.82
Peak 10 g average SAR (W/kg)	0.44	0.54	0.44
Whole-head SAR (W/kg)	0.015	0.016	0.015
Mobile phone - 1748 MHz			
	Head no electrodes	Set 1 32 electrodes/leads	Set 2 32 electrodes/leads
Net input power (W)	0.13	0.13	0.13
Power dissipated (W)	0.11	0.10	0.10
Radiation efficiency	23.130%	18.400%	19.4%
Impedance (Z)	16.8 + j121	15.82 + j120	16.03 + j120.7
Peak 1 g average SAR (W/kg)	0.19	0.21	0.20

Dipole - 915 MHz			
	Head no electrodes	**Set 1 32 electrodes/leads**	**Set 2 32 electrodes/leads**
Peak 10 g average SAR (W/kg)	0.10	0.11	0.10
Whole-head SAR (W/kg)	0.002	0.002	0.002

TABLE 4

Variable Number of Electrodes

Mobile phone - 915 MHz			
	Head no electrodes	**Set 1 19 electrodes/leads**	**Set 2 32 electrodes/leads**
Net input power (W)	0.25	0.25	0.25
Power dissipated (W)	0.19	0.21	0.21
Radiation efficiency	21.9%	17.2%	17.1%
Impedance (Z)	64.08 + j124.33	67.84 + j129.18	68 + j129.35
Peak 1 g average SAR (W/kg)	0.82	0.86	0.86
Peak 10 g average SAR (W/kg)	0.44	0.53	0.54
Whole-head SAR (W/kg)	0.015	0.016	0.016

Notes. Head model with 19 and 32 EEG electrodes leads, with leads bundled as in Set 1. RF-field source was mobile phone at 915 MHZ. SARs are normalized to net input power equal to 0.25 W.

TABLE 5

Variable Resistivity

Mobile phone - 915 MHz			
	Head no electrodes	**Set 1 32 electrodes/leads ρ = 0.01 Ωm**	**Set 2 32 electrodes/leads ρ = 0.01 Ωm**
Net input power (W)	0.25	0.25	0.25
Power dissipated (W)	0.19	0.20	0.20
Radiation efficiency	21.9%	21.1%	21.7%
Impedance (Z)	64.08 + j124.33	201 + j0.954	62.24 + j125.27
Peak 1 g average SAR (W/kg)	0.82	0.83	0.79
Peak 10 g average SAR (W/kg)	0.44	0.49	0.44
Whole-head SAR (W/kg)	0.015	0.016	0.015